ELECTRICAL ENGINEERING

10.1126/sciadv.1400198

Rationally designed graphene-nanotube 3D architectures with a seamless nodal junction for efficient energy conversion and storage

Yuhua Xue,[1,2] Yong Ding,[3] Jianbing Niu,[4] Zhenhai Xia,[4] Ajit Roy,[5] Hao Chen,[2] Jia Qu,[2] Zhong Lin Wang,[3,6]* Liming Dai[1,2]*

One-dimensional (1D) carbon nanotubes (CNTs) and 2D single-atomic layer graphene have superior thermal, electrical, and mechanical properties. However, these nanomaterials exhibit poor out-of-plane properties due to the weak van der Waals interaction in the transverse direction between graphitic layers. Recent theoretical studies indicate that rationally designed 3D architectures could have desirable out-of-plane properties while maintaining in-plane properties by growing CNTs and graphene into 3D architectures with a seamless nodal junction. However, the experimental realization of seamlessly-bonded architectures remains a challenge. We developed a strategy of creating 3D graphene-CNT hollow fibers with radially aligned CNTs (RACNTs) seamlessly sheathed by a cylindrical graphene layer through a one-step chemical vapor deposition using an anodized aluminum wire template. By controlling the aluminum wire diameter and anodization time, the length of the RACNTs and diameter of the graphene hollow fiber can be tuned, enabling efficient energy conversion and storage. These fibers, with a controllable surface area, meso-/micropores, and superior electrical properties, are excellent electrode materials for all-solid-state wire-shaped supercapacitors with poly (vinyl alcohol)/H_2SO_4 as the electrolyte and binder, exhibiting a surface-specific capacitance of 89.4 mF/cm^2 and length-specific capacitance up to 23.9 mF/cm, — one to four times the corresponding record-high capacities reported for other fiber-like supercapacitors. Dye-sensitized solar cells, fabricated using the fiber as a counter electrode, showed a power conversion efficiency of 6.8% and outperformed their counterparts with an expensive Pt wire counter electrode by a factor of 2.5. These novel fiber-shaped graphene-RACNT energy conversion and storage devices are so flexible they can be woven into fabrics as power sources.

INTRODUCTION

Carbon nanomaterials, including one-dimensional (1D) carbon nanotubes (CNTs) and 2D single-atomic layer graphene, have been demonstrated to show superior thermal, electrical, and mechanical properties. Because of the presence of strong covalent bonding in the carbon plane and the much weaker van der Waals interaction in the transverse direction between the layers, these 1D and 2D nanomaterials exhibit strong direction-dependent thermal and electrical transport properties with extremely low out-of-plane conductivities due to the weak interlayer van der Walls interaction. However, many practical applications require high through-thickness thermal and electrical conductivities. Recent theoretical studies (*1*, *2*) have indicated that 3D carbon architectures, particularly a 3D pillared structure, consisting of parallel graphene layers supported by vertically aligned CNTs (VACNTs) in between, have desirable out-of-plane transport and mechanical properties while maintaining the excellent properties of their building blocks. A few groups have tried to prepare multilayered 3D graphene-CNT pillared structures (*3*–*7*). However, most of the reported preparation methods involved multiple steps and/or chemical vapor deposition (CVD) with metal nanoparticle catalysts, which could cause detrimental effects on the interfacial mechanical and transport properties. So far, 3D graphene-CNT network with a covalently bonded pure carbon-carbon junction at the graphene-CNT interface has rarely been experimentally demonstrated. To ensure that the 3D graphene-CNT structures have efficient thermal/electrical transport characteristics in all directions, it is necessary to create a seamless pure C-C nodal junction between the constituent graphene sheets and CNTs. In this study, we developed a novel one-step CVD method without an additional metal nanoparticle catalyst to directly grow hollow fibers made of radially aligned CNT (RACNT) arrays bounded by cylindrical graphene layers with covalently bonded seamless pure C-C nodal junctions between the graphene and RACNTs (Figs. 1D and 2). Different from other types of carbon fibers [for example, CNT fibers or graphene fibers (*8*–*13*)], these novel 3D graphene-RACNT fibers have rationally designed 3D micro-/mesoporous architectures with a large surface area [Brunauer-Emmett-Teller (BET) surface area, 526.91 m^2/g] and minimized interfacial electrical/thermal resistances. Furthermore, the 3D graphene-RACNT structure acts as an ideal electrode material for super-efficient energy storage, with an area capacitance and a length capacitance (capacitance per unit length) as high as 89.4 mF/cm^2 and 23.9 mF/cm, respectively, both of which are one to four times the corresponding record-high capacities reported for other fiber-like supercapacitors (table S1). Moreover, dye-sensitized solar cells (DSSCs) with the 3D graphene-RACNT fiber as a counter electrode to replace Pt showed a power conversion efficiency up to 6.8%, which outperformed the DSSC using CNT fiber, graphene fiber, and even Pt wire as a counter electrode (table S2), indicating synergistic effects of the 3D architecture.

[1]Center of Advanced Science and Engineering for Carbon (Case4Carbon), Department of Macromolecular Science and Engineering, Case Western Reserve University, Cleveland, OH 44106, USA. [2]Institute of Advanced Materials for Nano-Bio Applications, School of Ophthalmology & Optometry, Wenzhou Medical University, Wenzhou, Zhejiang 325027, China. [3]School of Materials Science and Engineering, Georgia Institute of Technology, Atlanta, GA 30332–0245, USA. [4]Department of Materials Science and Engineering, University of North Texas, Denton, TX 76203, USA. [5]Materials and Manufacturing Directorate, Air Force Research Laboratory, Dayton, OH 45433 USA. [6]Beijing Institute of Nanoenergy and Nanosystems, Chinese Academy of Sciences, Beijing 100083, China.
*Corresponding author. E-mail: zhong.wang@mse.gatech.edu (Z.L.W.); liming.dai@case.edu (L.D.)

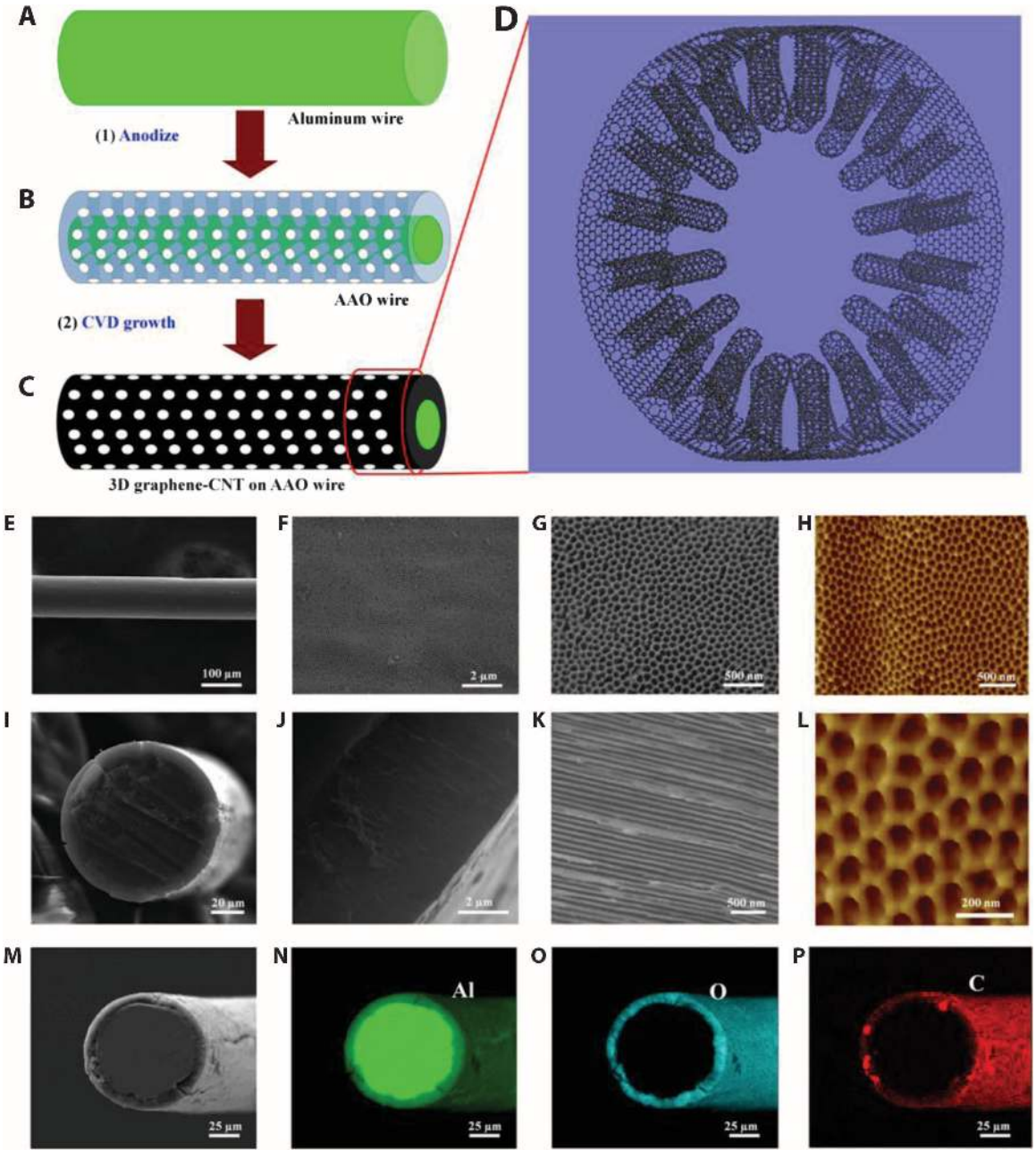

Fig. 1. Schematic diagrams showing the synthesis and microstructures of a 3D graphene-RACNT fiber. (**A**) Aluminum wire. (**B**) Surface anodized aluminum wire (AAO wire). (**C**) 3D graphene-RACNT structure on the AAO wire. (**D**) Schematic representation of the pure 3D graphene-RACNT structure. (**E** to **G**) Top view SEM images of the 3D graphene-RACNT fiber at different magnifications. (**I** to **K**) SEM images of the cross-section of the 3D graphene-RACNT fiber. (**H** and **L**) AFM images of the 3D graphene-RACNT fiber. (**M** to **P**) SEM image (M) and corresponding EDX elemental mapping of (N) aluminum, (O) oxygen, and (P) carbon from the 3D graphene-RACNT fiber.

RESULTS AND DISCUSSION

The synthetic route to the 3D graphene-RACNT hollow fibers is shown in Fig. 1 (A to C). To start with, an aluminum wire (purity >99.99%, Alfa Aesar) was anodized in 0.3 M oxalic acid solution at 40 V and 3°C to convert the outside surface of an aluminum wire into an anodized aluminum oxide (AAO) shell (step 1, Fig. 1, A and B). The thickness of the resulting AAO shell can be regulated by changing the anodizing time. Thus, a prepared wire with aluminum core and AAO shell (AAO wire) was then used as a template for a single-step CVD deposition without additional metal nanoparticle catalyst to produce the 3D graphene fiber sheathed with RACNTs (step 2, Fig. 1, B and C). Upon CVD deposition, the color of the template wire changed from white to black (fig. S1), indicating the formation of a graphitic carbon layer over the template surface, including the inner holes of the AAO shell, to produce the 3D RACNTs sheathed with graphene, as schematically

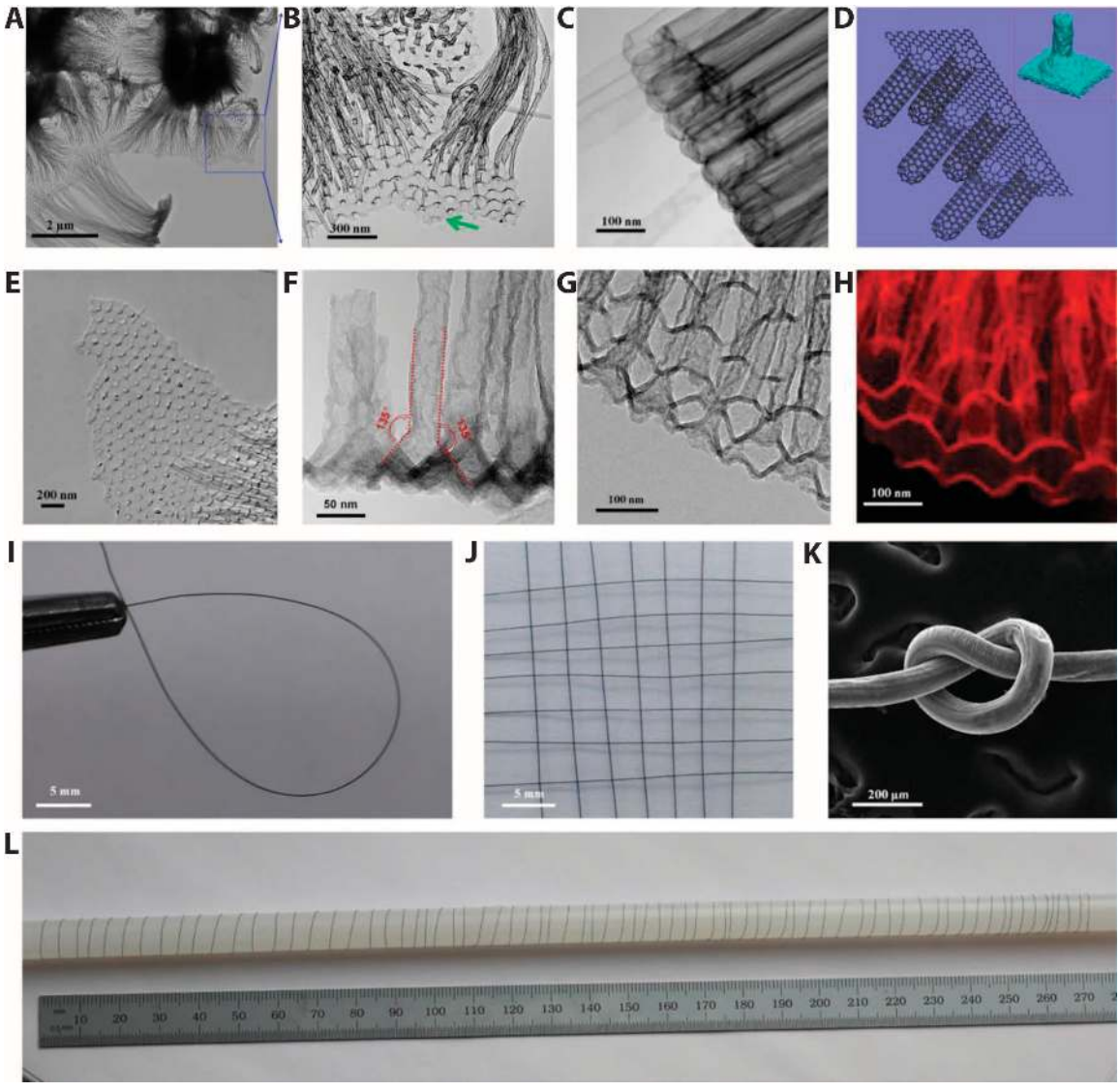

Fig. 2. Microscopy characterization of the 3D graphene-RACNT structures. (**A** and **B**) Graphene sheet connecting to the open tips of RACNTs. (**C**) Closed end of RACNTs. (**D**) Schematic representation of the 3D graphene-RACNT network; inset shows the energy-minimized structure from MD simulations (Supplementary Materials). (**E**) Broken graphene sheet from the 3D graphene-RACNT network. (**F**) TEM image of the side view of the 3D graphene-RACNT around the graphene-nanotube interface. (**G** and **H**) Cross-section view of the constituent RACNTs within the 3D graphene-RACNT structure (G) and corresponding carbon mapping (H). (**I**) Circle-shaped 3D graphene-RACNT fiber. (**J**) Piece of weaved graphene-RACNT fibers. (**K**) SEM image of a knot of the graphene-RACNT fiber. (**L**) Photograph of a 2-m-long graphene-RACNT fiber rolled on a long stick. [The diameter of the graphene-RACNT fibers in (I) to (L) is 100 μm.]

shown in Fig. 1D. The length of the 3D hierarchically structured graphene-RACNT fiber thus produced is, in principle, only limited by the length of the aluminum wire as the starting material, which can be commercially produced in a continuous extrusion process to allow for a large-scale production of the 3D graphene-RACNT fibers. Because of the one-step CVD growth, covalently bonded seamless C-C nodal junctions between the graphene and the RACNTs were realized to ensure efficient thermal/electrical transport characteristics for the 3D graphene-RACNT structures. The open ends of the RACNTs on the fiber surface could not only provide a large surface area but also allow for efficient diffusions of electrolytes to and from the constituent nanotubes. These unique structural features make our graphene-RACNT fibers attractive for a wide range of potential applications, ranging from wearable electronics to energy conversion and storage devices, as exemplified by ultraperformance supercapacitors and DSSCs developed in this study.

The structures of the 3D graphene-RACNT fibers were systematically characterized using microscopy techniques. Figure 1E reproduces a typical low-magnification scanning electron microscopy (SEM) image for the as-prepared 3D graphene-RACNT fiber, which shows a homogenous diameter of ~100 μm along the fiber length. Under higher magnifications, opened tips of the "buried" RACNTs are evident (Fig. 1, F and G). The hole diameter seen in the SEM image (Fig. 1G) is in good agreement with that seen in an atomic force microscopy

(AFM) image shown in Fig. 1H and can be estimated from the AFM image to be about 50 nm, which is in consistent with the corresponding hole diameter of the AAO template (Fig. 1L). Figure 1 (I to K) shows the SEM images of the cross-section of the 3D graphene-RACNT fiber under different magnifications.

As can be seen in Fig. 1I, the unanodized aluminum core is surrounded by the ~6 μm-thick 3D graphene-RACNT shell, which is the same as the RACNT length and depends mainly on the anodized time. The SEM images of the cross-section of the shell under higher magnifications show the presence of well-aligned CNTs (Fig. 1, J and K). The corresponding energy-dispersive x-ray spectroscopic (EDX) elemental mapping shows the presence of carbon on the fiber surface and through-thickness within the shell (Fig. 1P), indicating the formation of the 3D graphene-RACNT fiber (cf. Fig. 1D). Figure 1 (N to P) further shows that the center of the fiber is only composed of Al (Fig. 1N), whereas the shell is composed of Al (Fig. 1N) and O (Fig. 1O) in addition to C (Fig. 1P). Thus, the EDX mapping reveals that carbon has been successfully deposited into the AAO holes within the shell of the template fiber and its surface to produce the 3D seamlessly bonded graphene-RACNT structure, as schematically shown in Fig. 1D.

By removing the aluminum and aluminum oxide in the 1 M KOH solution, we obtained the neat hollow 3D graphene-RACNT fiber with big graphene tube sheathing RACNT arrays along its inner surface (fig. S2). Figure 2 (A to H) shows the transmission electron microscopy (TEM) images of the 3D graphene-RACNT fiber after removal of the aluminum and aluminum oxide template. As can be seen in Fig. 2A, the RACNTs were connected to a graphene sheet of homogeneously distributed open holes (Fig. 2B and movie S1), consistent with the SEM (Fig. 1G) and AFM (Fig. 1, H and L) images shown in Fig. 1. The graphene edge can be observed in Fig. 2B, as indicated by the green arrow, and also in Fig. 2E for a small piece of the edge broken off from the graphene-RACNT sample. More TEM images from the end and side wall of the 3D graphene-RACNT fiber can be found in figs. S3 and S4, respectively. The nanotube bundles seen in Fig. 2A and fig. S4A from the TEM images for broken pieces were caused by the surface energy–induced bundling (*14*) during the template removal, whereas the integrity of the 3D graphene-RACNT structure could be largely retained by the sheathed graphene "tube" intimately connected with the open end of the constituent RACNTs, as shown in figs. S2D and S4D. The integrity of the 3D graphene-RACNT structure can be further observed by dynamically rotating the TEM samples from −19° to 30° (fig. S5 and movie S2). The TEM images for the other end of the RACNT array are given in Fig. 2C, showing that the nanotube end tips away from the graphene sheet in the 3D graphene-RACNT fiber were all closed (Fig. 2C). These TEM images are consistent with the 3D graphene-RACNT network schematically drawn in Fig. 2D, which acts as a building block to form the 3D graphene-RACNT hollow fiber, as schematically shown in Fig. 1D and supported by the SEM and AFM images in Fig. 1. Also included in the inset of Fig. 2D is the energy-minimized graphene-CNT junction from the molecular dynamic (MD) simulations (see below and the Supplementary Materials). As expected, Fig. 2D shows that the open end for each of the constituent RACNTs was seamlessly connected to the graphene sheet. The TEM image of the cross-section view of the 3D graphene-RACNT structure given in Fig. 2F counterintuitively shows a connecting angle about 135° (instead of 90°) at the graphene-RACNT interface. Figure 2 (G and H) reproduces the TEM images and the electron energy loss spectrum elemental mapping of carbon from the same part of a 3D graphene-RACNT network, respectively. The seamless carbon-carbon nodal junction was revealed by using electron tomography recorded in TEM mode. By tilting the junction structure continuously from −70° to 70° at 1° per step, a total of 141 TEM images were recorded from the junction, by which the 3D structure was reconstructed. A movie made from those consequent TEM images can reveal the seamless 3D junction structure between the CNTs and the graphene sheet (movies S1 and S2). The observed ~135° connecting angle is further confirmed by energy minimization and MD simulations described in the Supplementary Materials. Figure S6 reproduces a TEM image of an individual CNT from the graphene-RACNT fiber, which shows a reasonably well-graphitized nanotube structure with an outer diameter of ~50 nm and about 15 concentric carbon shells.

Figure S7 shows a typical Raman spectrum of the as-prepared 3D graphene-RACNT fiber. As can be seen, the D band at 1350 cm^{-1} is relatively weak with respect to the G band at 1595 cm^{-1}, indicating a reasonably high graphitization degree for the whole fiber sample. The weak 2D band over 2700 cm^{-1} suggests the presence of graphene, although RACNT signals are dominant, as also indicated by Figs. 1D and 2F. The x-ray photoelectron spectroscopy (XPS) spectra of the 3D graphene-RACNT fiber are given in fig. S8, which also shows a main carbon peak, along with small Al and O peaks from the AAO template. The high-resolution XPS C1s spectrum shows a sharp peak at 284.5 eV, which is attributed to the sp^2 C-C bond from graphitic carbons (*15*, *16*).

Although the as-prepared AAO wire was electrically insulating, it became highly conductive (16 ohms/cm) after being deposited with the 3D graphene-RACNT structure (fig. S9). The as-prepared 3D graphene-RACNT fiber was also sufficiently flexible to be bent from a straight line into a circle (Fig. 2I) and to be made into a piece of weave with potentials for electronic textile applications (Fig. 2J). Similar to other CNT or graphene fibers (*8*–*13*), our 3D graphene-RACNT fibers can also be knotted (Fig. 2K) or rolled along a long stick (Fig. 2L).

The as-prepared 3D graphene-RACNT fibers with high conductivity, good mechanical property, and pinhole-free coverage on the AAO template were found to be attractive electrodes for fiber-like supercapacitors. The electrochemical performance of the 3D graphene-RACNT fiber was first evaluated in a three-electrode cell in 1 M H_2SO_4 (fig. S10). Several different graphene-RACNT fiber electrodes with different shell thicknesses (fig. S11) were also investigated. Figure S12 shows that their electroactive surface areas, and hence supercapacitances (fig. S13), increased with increasing anodization time (fig. S12 and table S3). To further enlarge the electroactive surface area, another two large-diameter aluminum wires (380 and 810 μm) were selected (figs. S14 and S15). The cyclic voltammogram (CV) curves of these three fibers are shown in fig. S16A, which reveals a much higher current density for fiber-810 than for fiber-380 and fiber-100. Nevertheless, fiber-100 has the lowest resistance of about 1.4 ohms (fig. S16B and table S4).

Figure 3 (A and B) shows the SEM images of a solid-state wire-like supercapacitor based on two twisted 3D graphene-RACNT fiber electrodes sandwiched with poly(vinyl alcohol) (PVA)/H_2SO_4 gel as the solid electrolyte and binder. The CVs measured from the solid-state wire supercapacitor at different scanning rates from 100 to 500 mV/s all show a regular rectangular shape (Fig. 3C), indicating an ideal capacitive behavior with a high-rate capability. The CV curve is still somewhat rectangular in shape even at the ultrahigh scan rate up to 50 V/s (fig. S17A) because of the ultralow resistance (fig. S16B and table S4). Furthermore, the newly developed wire supercapacitor could

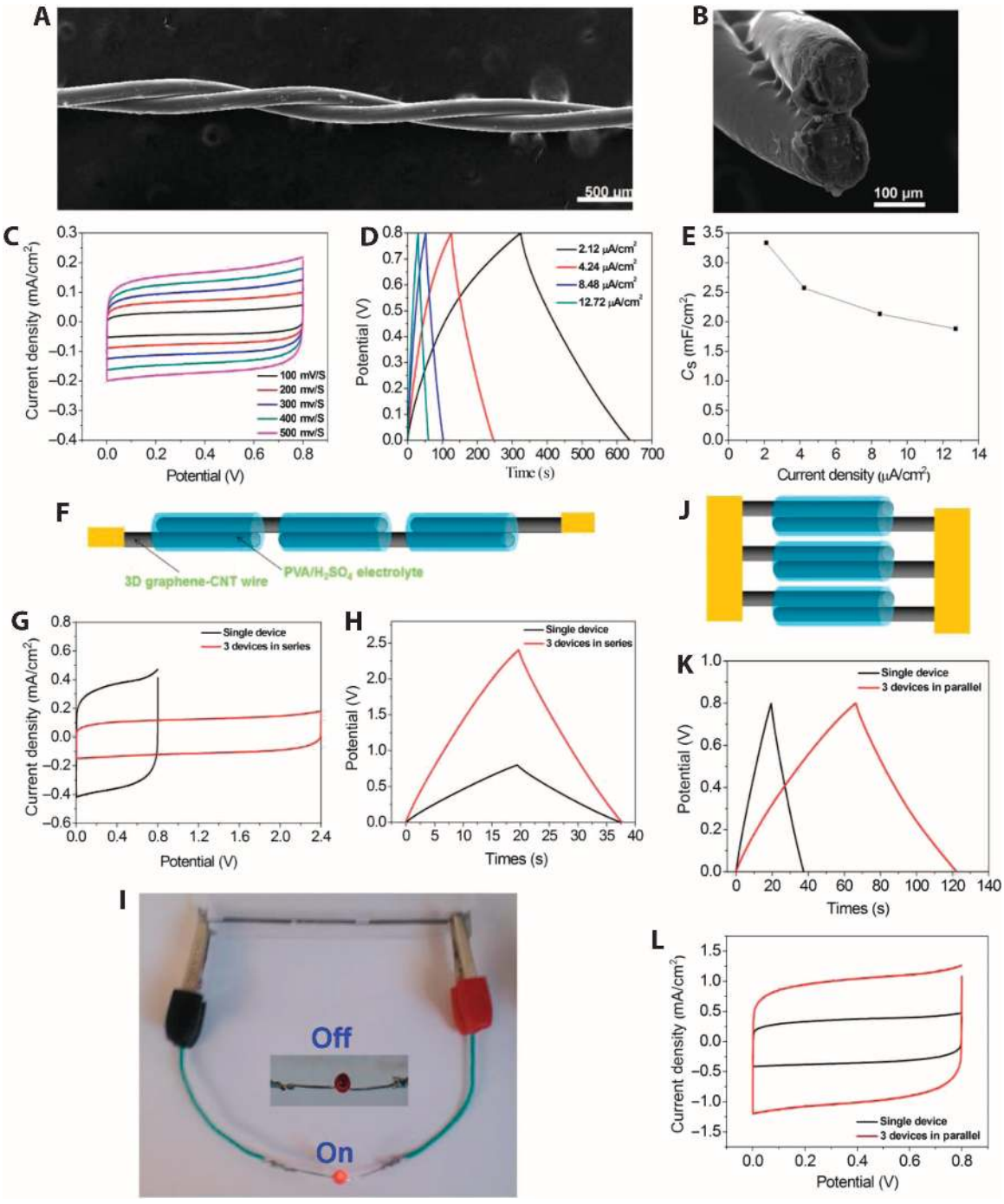

Fig. 3. Performance of the solid wire supercapacitors of 3D graphene-CNT fiber for energy storage. (**A** and **B**) SEM images of the top and cross-section of the solid-state wire supercapacitor based on the 3D graphene-RACNT fiber electrodes (the diameter of the fiber is 100 μm). (**C**) CV curves of the solid-state wire supercapacitor based on the 3D graphene-RACNT wire electrodes at scanning rates from 100 to 500 mV/s. (**D**) Galvanostatic charge and discharge curves of the 3D graphene-RACNT wire capacitor at different currents. (**E**) Surface-specific capacitance of the 3D graphene-RACNT wire electrode calculated from the galvanostatic charge/discharge curves. (**F** to **L**) Integrated solid wire supercapacitors either in series or in parallel (the diameter of the fibers used in integrated devices is 380 μm). (F) Schematic representation of an integrated supercapacitor in series from three graphene-RACNT wire supercapacitors. (G and H) Galvanostatic charge-discharge curves and CV curves, respectively, for the series integrated graphene-RACNT wire supercapacitor and a single wire supercapacitor. (I) Use of an integrated supercapacitor to light up a commercial LED. (J) Schematic representation of an integrated supercapacitor in parallel from three graphene-RACNT wire supercapacitors. (K and L) Galvanostatic charge-discharge curves and CV curves, respectively, for the parallel integrated graphene-RACNT wire supercapacitor and a single wire supercapacitor.

be charged and discharged at either high (fig. S17B) or low current densities (Fig. 3D). The galvanostatic charge/discharge curves measured at high current densities from 424 to 2120 μA/cm^2 are nearly symmetric straight lines (fig. S17B), indicating an ideal double-layer supercapacitor behavior. Even at a very low current density of 2.12 μA/cm^2, the galvanostatic charge/discharge curve shows a triangular shape (Fig. 3D). From the galvanostatic charge/discharge curve, a specific capacitance of ~3.33 mF/cm^2 was calculated at the discharge current of 2.12 μA/cm^2 for the solid-state wire supercapacitor based on the 3D graphene-RACNT fiber electrodes. The specific capacitance was found to decrease with increasing current density (Fig. 3E). By using the 810-μm-thick aluminum wire after a prolonged anodization (120 hours) as the electrodes, we can further increase capacitance of the solid-state 3D graphene-RACNT fiber supercapacitor. In fig. S18, a record-high surface-specific capacitance up to 89.4 mF/cm^2 was obtained for the 3D graphene-RACNT fiber (810 μm), which is much higher than the capacitance of wire supercapacitors made from ZnO nanorods (2 mF/cm^2) (*17*), CNT fibers (0.6 mF/cm^2) (*18*), and graphene fibers (1.7 mF/cm^2) (*19*), and even higher than that of the PEDOT [poly(3,4-ethylenedioxythiophene)]–coated CNT fibers (73 mF/cm^2) (*20*). The length-specific capacitance of the 3D graphene-RACNT wire (810 μm) supercapacitor is as high as 23.9 mF/cm, which is almost 1000 times that of the CNT fibers (0.024 mF/cm) (*18*) and graphene fibers (0.02 mF/cm) (*19*) and even 50 times higher than that of the PEDOT-coated CNT capacitors (0.46 mF/cm) (*20*). Although some more advanced capacitors have been reported in recent years (*21*–*23*), our 3D graphene-RACNT wire capacitor is still among the best.

The newly developed solid-state wire supercapacitor based on the graphene-RACNT electrodes was further subjected to a long-term stability test. As can be seen in fig. S19A, there was no obvious change even after about 10,000 consecutive charge/discharge cycles, indicating excellent long-term device stability. Moreover, the 3D graphene-RACNT wire supercapacitor also showed high flexibility, wherein it could be easily rolled over a glass tube without any noticeable effect on the device performance (fig. S20). Figure S19B shows bending cycle stability measured for the 3D graphene-RACNT supercapacitor over 100 times at bending angles up to 90°, indicating very good stability with about 90% capacitance retention over bending for 100 times.

Having demonstrated superb performance for the solid-state 3D graphene-RACNT wire supercapacitor, we have further integrated individual 3D graphene-RACNT wire supercapacitors into assemblies either in series or in parallel to meet specific energy needs for diverse practical applications. Figure 3 (F and I) shows three wire supercapacitors connected in series. As expected, the charge/discharge voltage window of the three graphene-RACNT wire supercapacitors connected in series is about three times of that for a single wire supercapacitor

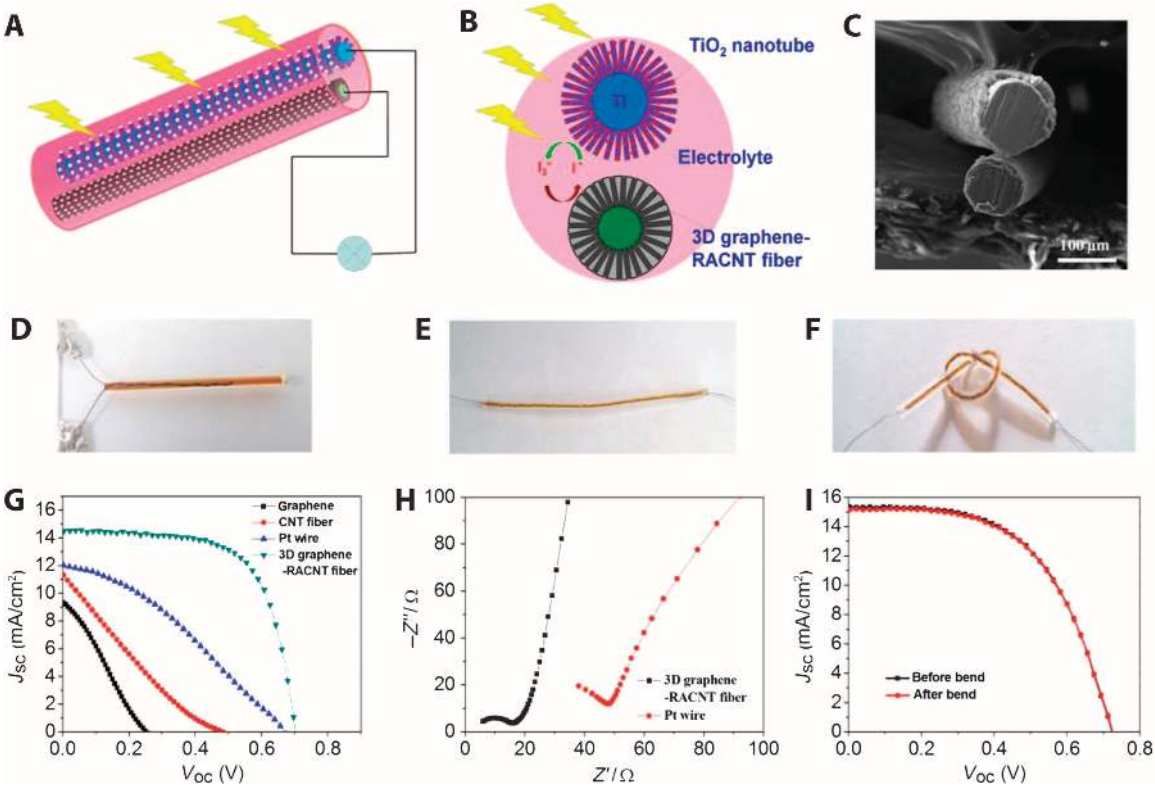

Fig. 4. 3D graphene-RACNT fiber as the counter electrode for wire-shaped DSSCs. (**A**) Schematic representation of wire-shaped DSSC using 3D graphene-CNT fiber as the counter electrode and the TiO_2 nanotube fiber as the photo anode. (**B**) Schematic drawing for the cross-section view of the wire-shaped DSSC. (**C**) SEM image of the cross-section view of the wire-shaped DSSC. (**D**) Photograph of the wire-shaped DSSC sealed in a glass capillary tube. (**E**) Flexible wire-shaped DSSC sealed in a transparent FET plastic tube. (**F**) Knot made from the flexible DSSC. (**G**) Current density–voltage characteristics of DSSCs with graphene wire, CNT wire, Pt wire, or 3D graphene-RACNT fiber as the counter electrode. (**H**) Nyquist plots of the 3D graphene-CNT fiber and the Pt wire measured in the I^-/I_3^- electrolyte (10 mM LiI + 1 mM I_2 + 0.1 M $LiClO_4$ + acetonitrile). (**I**) Current density–voltage characteristics of DSSCs with the 3D graphene-RACNT wire counter electrode before and after bending.

(Fig. 3, G and H) with an almost identical discharge time. The integrated devices can be used as a power source, as exemplified in Fig. 3I, to light up a commercial LED (Red LED, 1.9 to 2.0 V, from Microtivity). As can be seen in Fig. 3 (J to L), the output current density and the discharge time for three graphene-RACNT wire supercapacitors connected in a parallel configuration are about three times of those for a single wire supercapacitor. These results show the scalability of the 3D graphene-RACNT wire supercapacitors. To further demonstrate the potential applications for the newly developed all-solid-state graphene-RACNT wire supercapacitors as efficient energy storage components for wearable devices, we weaved the 3D graphene-RACNT wire supercapacitors into fabrics (fig. S21A). These wire capacitors weaved into fabrics could be used as flexible power sources without detrimental effect on their performance.

The 3D graphene-RACNT fiber could also be used as an efficient counter electrode in DSSCs to replace the expensive Pt while still retaining and even exceeding the high performance of the Pt-based DSSCs. In Fig. 4 (A and B), the wire-shaped DSSC was fabricated by twining a titanium wire sheathed with vertically aligned titanium oxide (TiO_2) nanotubes (fig. S22) as the photoanode with the graphene-RACNT counter electrode (Fig. 4C), which was sealed in a capillary tube containing the I^{3-}/I^- electrolyte solution (Fig. 4D) (*24*, *25*). The performance of the wire-shaped DSSC thus prepared was evaluated under standard illumination (AM 1.5, 100 mW/cm^2). Figure 4G shows the current density–voltage (*J*-*V*) characteristics with the corresponding numerical data listed in table S2. As can be seen, the wire-shaped DSSC with a 3D graphene-CNT fiber counter electrode exhibited a short-circuit current (J_{sc}) of 14.50 mA/cm^2, an open-circuit voltage (V_{oc}) of 0.70 V, and a fill factor (*FF*) of 0.67. The overall power conversion efficiency is as high as 6.80%, which is much higher than that of its counterparts with the Pt wire (2.74%), graphene wire (0.63%), or CNT wire (1.14%) as the counter electrode (Fig. 4G and table S2). The series resistance and charge transfer resistance of the 3D graphene-RACNT fiber are much smaller than those of the Pt wire (Fig. 4H). Compared with a pure graphene electrode, the 3D graphene-RACNT fiber electrode has rationally designed 3D micro-/mesoporous architectures with a large surface area and a seamless nodal junction at the graphene and RACNT interface. Thus, the 3D graphene-RACNT fiber electrode provides enormous graphitic surface area to speed the I_3^-/I^- reaction, the 3D micro-/mesoporous architectures to facilitate the reactants and electrolyte diffusion, and the seamless nodal junction to minimize the interfacial electrical/thermal resistances, which significantly enhanced the device performance. Flexible wire-shaped DSSCs can also be prepared by sealing the electrodes in a transparent fluorinated ethylene propylene (FET) tube (Fig. 4E), which is sufficiently flexible to be made into a knot (Fig. 4F). Bending the flexible DSSC shown in fig. S23 did not cause any obvious change in its performance (Fig. 4I and table S5). Because of its versatile and scalable nature, the methodologies developed in this study could be applicable to the scalable production of other 3D hierarchically structured multifunctional materials for a wide range of applications.

MATERIALS AND METHODS

Preparation of the AAO wire

Three different aluminum wires (purity > 99.99%) with diameters of 13, 100, 380, and 810 μm were purchased from Alfa Aesar Company. Before use, the aluminum wire was washed in acetone for 10 min and was then anodized by a two-step electrochemical process, as previously described (*26*, *27*). In a typical experiment, aluminum wires were anodized in 0.3 M oxalic acid solution at 3°C and 40 V. The first anodizing step took 1 hour. The aluminum oxide layer was removed in the mixture solution of 6 wt % phosphoric acid and 1.8 wt % chromic acid at 60°C for 4 hours. The second anodizing step lasted for 2 to 120 hours depending on the desirable thicknesses for the AAO shell. The pores in the AAO shell were finally widened in 0.1 M phosphoric acid solution for 40 min.

Synthesis of the 3D graphene-RACNT fiber on the AAO wire

The 3D graphene-RACNT fiber was grown on the AAO wire by using a one-step CVD process. Typically, the AAO wire was put inside a quartz tube furnace. The furnace was heated up to 620°C with argon gas continuously flowing at a rate of 200 SCCM (standard cubic centimeter per minute). At 620°C, acetylene gas (20 SCCM) and hydrogen (10 SCCM) were introduced to the furnace. The sample was kept in the furnace under these conditions for 55 min to achieve the one-step growth of the 3D graphene-RACNT fiber on the AAO wire. Upon completion of the growth process, the 3D graphene-RACNT fiber was rapidly moved away from the furnace center (620°C), and the quartz tube was air-cooled down to room temperature. Thereafter, the 3D graphene-RACNT fiber was taken out from the quartz tube for characterization and was directly used as the wire electrode without any further treatment unless otherwise stated.

Fabrication of the solid-state wire supercapacitor

The PVA/H_2SO_4 gel was used as the solid electrolyte, which was prepared as follows: 2.2 g of PVA (weight-average molecular weight, 85,000 to 124,000; Sigma-Aldrich) powder was added into 20 ml of water, followed by heating at 90°C under vigorous stirring, and then 2.2 g of H_2SO_4 was added after the PVA solution became clear.

For supercapacitor construction, the 3D graphene-RACNT fibers were precoated with a layer of PVA/H_2SO_4 gel and then dried at room temperature for 1 hour. The flexible solid-state wire supercapacitor was then fabricated by intertwisting two of the 3D graphene-RACNT fiber electrodes together.

The surface-specific capacitance for the solid-state wire capacitance was calculated from the galvanostatic charge and discharge curves by using the following equation:

$$C_s = 4I\Delta t/(SV),$$

where I is the applied current, Δt is the discharge time, S is the surface area of the graphene-RACNT wire electrodes, and V is the potential range.

The corresponding length-specific capacitance was calculated from the galvanostatic charge and discharge curves using the following equation:

$$C_L = 4I\Delta t/(LV),$$

where L is the length of the graphene-CNT wire electrodes.

The surface- and length-specific capacitances for the three-electrode supercapacitor in H_2SO_4 were calculated from the galvanostatic charge and discharge curves using the following equations:

$$C_s = I\Delta t/(SV) \text{ and } C_L = I\Delta t/(LV).$$

Fabrication of the wire DSSC

The aligned TiO_2 nanotube/Ti wire was prepared by electrochemical anodizing of titanium wire (diameter of 127 μm, purity of 99.99%; Alfa Aesar) in 0.3 wt % NH_4F/ethylene glycol solution containing 2 v % H_2O at voltages of 60 V for 5.5 hours (*28*). After being washed with deionized water, the resulting TiO_2 nanotube/Ti wire was then annealed at 500°C in air for 1 hour. The annealed wire was further treated with 40 mM $TiCl_4$ solution at 70°C for 30 min, followed by annealing at 450°C in air for 30 min. The TiO_2 nanotube/Ti wire was immersed in a mixture solvent of acetonitrile and isobutanol (1:1, v/v) solution containing 0.5 mM N719 dye (Solaronix) for 24 hours to form the sensitized wire photoanode. The wire-shaped DSSC cell was fabricated by packaging the aligned TiO_2 nanotube/Ti wire photoanode and the 3D graphene-RACNT fiber counter electrode in a capillary tube or transparent FET tube (purchased from Amazon) containing the electrolyte of 0.6 M dimethyl-3-propylimidazolium iodide, 0.04 M I_2, 0.02 M LiI, 0.1 M guanidine thiocyanate, and 0.5 M 4-terbutylpyridine in a mixture of acetonitrile and valeronitrile. To fabricate the reference DSSCs, the graphene wire was grown on the copper wire under 1000°C with methane as the carbon source and used as the counter electrode while the CNT fiber was obtained by dry spinning from VACNTs.

Characterization

The SEM images were recorded on a Hitachi SU8010 cold field emission SEM. SEM mapping was done on a Philips XL30 environmental scanning electron microscope. TEM was carried out using an FEI Tecnai F30 TEM working at 300 kV. The AFM images were obtained on an Agilent Technologies 5500 Scanning Probe Microscope. The XPS measurements were performed on a PHI 5000 VersaProbe. The Raman spectra were collected using a Raman spectrometer (Renishaw) with a 514-nm laser.

SUPPLEMENTARY MATERIALS

Supplementary material for this article is available at http://advances.sciencemag.org/cgi/content/full/1/8/e1400198/DC1

Fig. S1. Photographs of aluminum wire, AAO wire, and 3D graphene-RACNT deposited on the AAO wire.

Fig. S2. SEM images of the cross-section view of the 3D graphene-RACNT fiber after the removal of the aluminum and AAO template under different magnifications.

Fig. S3. TEM image of the edge of the 3D graphene-RACNT fiber with different magnifications.

Fig. S4. Top view TEM images of the center of the 3D graphene-RACNT fiber with different magnifications.

Fig. S5. TEM images of the side of the 3D graphene-RACNT fiber rotated with different angles from −19° to 30° around the red arrow.

Fig. S6. TEM images of an individual carbon nanotube from the 3D graphene-RACNT fiber under different magnifications.

Fig. S7. Raman spectrum of the 3D graphene-RACNT fiber on the AAO wire.

Fig. S8. The XPS survey spectrum of the 3D graphene-RACNT fiber, and the corresponding high-resolution XPS C1s spectrum.

Fig. S9. The resistance of the as-prepared 3D graphene-RACNT wire.

Fig. S10. CV curves and galvanostatic discharge curves of the 3D graphene-RACNT wire (0.1 mm in diameter) electrode in 1 M H_2SO_4 solution.

Fig. S11. SEM images of the 3D graphene-RACNT wire (100 μm in diameter) with different shell thicknesses via anodizing at different times.

Fig. S12. CV curves of the fiber-100μm-2hrs, fiber-100μm-4hrs, and fiber-100μm-12hrs in 5 mM $K_3Fe(CN)_6$/0.1 M KCl solution.

Fig. S13. CV curves, galvanostatic charge and discharge curves, and the surface specific capacitance of the 3D graphene-RACNT wire electrodes (fiber-100μm-2hrs, fiber-100μm-4hrs, and fiber-100μm-12hrs).

Fig. S14. Photographs of the 3D graphene-RACNT fibers prepared from aluminum wire with different diameters.

Fig. S15. SEM images of the 3D graphene-RACNT fibers prepared from aluminum wires with different diameters.

Fig. S16. CV curves and Nyquist plots of the 3D graphene-RACNT fibers with a diameter.

Fig. S17. CV curves of the solid-sate wire supercapacitor at high scanning rates, and galvanostatic charge and discharge curves of the 3D graphene-VACNT wire capacitor at high current density.

Fig. S18. Photograph, CV curves, galvanostatic charge and discharge curves, and the surface specific capacitance and length specific capacitance of the solid-state wire supercapacitor based on the 3D graphene-RACNT fiber electrodes (810 mm in diameter).

Fig. S19. The long term stability and bending stability tests for the supercapacitor based on the 3D graphene-RACNT electrodes with diameter of 100 μm.

Fig. S20. Photographs, CV curves, and galvanostatic charge/discharge curves of the 3D graphene-RACNT wire supercapacitor before and after rolling on a glass tube.

Fig. S21. Photographs of graphene-RACNT wire supercapacitor weaved into a piece of fabric and rolling over a stick, and its CV curves and galvanostatic charge/discharge curves before and after rolling on a stick.

Fig. S22. SEM images of TiO_2 nanotube/Ti wire.

Fig. S23. SEM images of a 3D graphene-RACNT flexible wire DSSC before and after bend.

Fig. S24. Schematics of Al_2O_3 template with a filleted hole in the center, and MD model of the template.

Fig. S25. Schematics of CNT-graphene junction.

Fig. S26. Side view and cross section of three-layered CNT-graphene junctions with 135° fillet and without fillet.

Fig. S27. Normalized bending energy predicted by the analytical model, and normalized potential energy calculated by MD as a function of the fillet angles.

Table S1. The reported areal capacitance and length capacitance of the fiber supercapacitor in references.

Table S2. J_{sc}, V_{oc}, FF, and power conversion efficiency for wire-shaped DSSCs with the 3D graphene-CNT fiber, and Pt wire as the counter electrode.

Table S3. Electroactive surface areas of the 3D graphene-RACNT fiber electrodes.

Table S4. Series resistance of the 3D graphene-RACNT fiber electrodes.

Table S5. J_{sc}, V_{oc}, FF, and power conversion efficiency for wire-shaped DSSCs with the 3D graphene-CNT fiber before and after bend.

Movie S1. A movie made from those consequent TEM images, showing the seamless 3D junction structure between the CNTs and the graphene sheet.

Movie S2. A movie made from those consequent TEM images, revealing the aligned CNT bundles (see text) and their seamless junction with the graphene sheet.

REFERENCES AND NOTES

1. V. Varshney, S. S. Patnaik, A. K. Roy, G. Froudakis, B. L. Farmer, Modeling of thermal transport in pillared-graphene architectures. *ACS Nano* **4**, 1153–1161 (2010).
2. G. K. Dimitrakakis, E. Tylianakis, G. E. Froudakis, Pillared graphene: A new 3-D network nanostructure for enhanced hydrogen storage. *Nano Lett.* **8**, 3166–3170 (2008).
3. Y. Zhu, L. Li, C. Zhang, G. Casillas, Z. Sun, Z. Yan, G. Ruan, Z. Peng, A.-R. Raji, C. Kittrell, R. H. Hauge, J. M. Tour, A seamless three-dimensional carbon nanotube graphene hybrid material. *Nat. Commun.* **3**, 1225 (2012).
4. F. Du, D. Yu, L. Dai, S. Ganguli, V. Varshney, A. K. Roy, Preparation of tunable 3D pillared carbon nanotube-graphene networks for high-performance capacitance. *Chem. Mater.* **23**, 4810–4816 (2011).
5. S. Li, Y. Luo, W. Lv, W. Yu, S. Wu, P. Hou, Q. Yang, Q. Meng, C. Liu, H.-M. Cheng, Vertically aligned carbon nanotubes grown on graphene paper as electrodes in lithium-ion batteries and dye-sensitized solar cells. *Adv. Energy Mater.* **1**, 486–490 (2011).
6. R. K. Paul, M. Ghazinejad, M. Penchev, J. Lin, M. Ozkan, C. S. Ozkan, Synthesis of a pillared graphene nanostructure: A counterpart of three-dimensional carbon architectures. *Small* **6**, 2309–2313 (2010).
7. C. Tang, Q. Zhang, M.-Q. Zhao, G.-L. Tian, F. Wei, Resilient aligned carbon nanotube/graphene sandwiches for robust mechanical energy storage. *Nano Energy* **7**, 161–169 (2014).
8. Y.-L. Li, I. A. Kinloch, A. H. Windle, Direct spinning of carbon nanotube fibers from chemical vapor deposition synthesis. *Science* **304**, 276–278 (2004).
9. K. Koziol, J. Vilatela, A. Moisala, M. Motta, P. Cunniff, M. Sennett, A. Windle, High-performance carbon nanotube fiber. *Science* **318**, 1892–1895 (2007).
10. N. Behabtu, C. C. Young, D. E. Tsentalovich, O. Kleinerman, X. Wang, A. W. K. Ma, E. A. Bengio, R. F. ter Waarbeek, J. J. de Jong, R. E. Hoogerwerf, S. B. Fairchild, J. B. Ferguson, B. Maruyama, J. Kono, Y. Talmon, Y. Cohen, M. J. Otto, M. Pasquali, Strong, light, multifunctional fibers of carbon nanotubes with ultrahigh conductivity. *Science* **339**, 182–186 (2013).
11. Z. Xu, C. Gao, Graphene chiral liquid crystals and macroscopic assembled fibre. *Nat. Commun.* **2**, 571 (2011).
12. M. D. Lima, S. Fang, X. Lepró, C. Lewis, R. Ovalle-Robles, J. Carretero-González, E. Castillo-Martínez, M. E. Kozlov, J. Oh, N. Rawat, C. S. Haines, M. H. Haque, V. Aare, S. Stoughton, A. A. Zakhidov, R. H. Baughman, Biscrolling nanotube sheets and functional guests into yarns. *Science* **331**, 51–55 (2011).

13. H. P. Cong, X. C. Ren, P. Wang, S. H. Yu, Wet-spinning assembly of continuous, neat, and macroscopic graphene fibers. *Sci. Rep.* **2**, 613 (2012).
14. H. Li, C.-L. Xu, G.-Y. Zhao, H.-L. Li, Effects of annealing temperature on magnetic property and structure of amorphous $Co_{49}Pt_{51}$ alloy nanowire arrays prepared by direct-current electrodeposition. *J. Phys. Chem. B* **109**, 3759–3763 (2005).
15. A. N. Sokolov, F. L. Yap, N. Liu, K. Kim, L. Ci, O. B. Johnson, H. Wang, M. Vosgueritchian, A. L. Koh, J. Chen, J. Park, Z. Bao, Direct growth of aligned graphitic nanoribbons from a DNA template by chemical vapour deposition. *Nat. Commun.* **4**, 2402 (2013).
16. M. A. Fanton, J. A. Robinson, C. Puls, Y. Liu, M. J. Hollander, B. E. Weiland, M. Labelle, K. Trumbull, R. Kasarda, C. Howsare, J. Stitt, D. W. Snyder, Characterization of graphene films and transistors grown on sapphire by metal-free chemical vapor deposition. *ACS Nano* **5**, 8062–8069 (2011).
17. J. Bae, M. K. Song, Y. J. Park, J. M. Kim, M. Liu, Z. L. Wang, Fiber supercapacitors made of nanowire-fiber hybrid structures for wearable/flexible energy storage. *Angew. Chem. Int. Ed.* **50**, 1683–1687 (2011).
18. T. Chen, L. Qiu, Z. Yang, Z. Cai, J. Ren, H. Li, H. Lin, X. Sun, H. Peng, An integrated "energy wire" for both photoelectric conversion and energy storage. *Angew. Chem. Int. Ed.* **51**, 11977–11980 (2012).
19. Y. Meng, Y. Zhao, C. Hu, H. Cheng, Y. Hu, Z. Zhang, G. Shi, L. Qu, All-graphene core-sheath microfibers for all-solid-state, stretchable fibriform supercapacitors and wearable electronic textiles. *Adv. Mater.* **25**, 2326–2331 (2013).
20. J. A. Lee, M. K. Shin, S. H. Kim, H. U. Cho, G. M. Spinks, G. G. Wallace, M. D. Lima, X. Lepró, M. E. Kozlov, R. H. Baughman, S. J. Kim, Ultrafast charge and discharge biscrolled yarn supercapacitors for textiles and microdevices. *Nat. Commun.* **4**, 1970 (2013).
21. D. T. Pham, T. H. Lee, D. H. Luong, F. Yao, A. Ghosh, V. T. Le, T. H. Kim, B. Li, J. Chang, Y. H. Lee, Carbon nanotube-bridged graphene 3D building blocks for ultrafast compact supercapacitors. *ACS Nano* **9**, 2018–2027 (2015).
22. H.-J. Peng, J.-Q. Huang, M.-Q. Zhao, Q. Zhang, X.-B. Cheng, X.-Y. Liu, W.-Z. Qian, F. Wei, Nanoarchitectured graphene/CNT@porous carbon with extraordinary electrical conductivity and interconnected micro/mesopores for lithium-sulfur batteries. *Adv. Func. Matter* **24**, 2772–2781 (2014).
23. D. Yu, K. Goh, H. Wang, L. Wei, W. Jiang, Q. Zhang, L. Dai, Y. Chen, Scalable synthesis of hierarchically structured carbon nanotube–graphene fibres for capacitive energy storage. *Nat. Nanotechnol.* **9**, 555–562 (2014).
24. Y. Xue, J. Liu, H. Chen, R. Wang, D. Li, J. Qu, L. Dai, Nitrogen-doped graphene foams as metal-free counter electrodes in high-performance dye-sensitized solar cells. *Angew. Chem. Int. Ed.* **51**, 12124–12127 (2012).
25. H. Wang, Y. H. Hu, Graphene as a counter electrode material for dye-sensitized solar cells. *Energy Environ. Sci.* **5**, 8182–8188 (2012).
26. H. Masuda, K. Fukuda, Ordered metal nanohole arrays made by a two-step replication of honeycomb structures of anodic alumina. *Science* **268**, 1466–1468 (1995).
27. M. J. Zheng, G. Li, X. Zhang, S. Huang, Y. Lei, L. Zhang, Fabrication and structural characterization of large-scale uniform SnO_2 nanowire array embedded in anodic alumina membrane. *Chem. Mater.* **13**, 3859–3861 (2001).
28. T. Chen, L. Qui, H. G. Kia, Z. Yang, H. Peng, Designing aligned inorganic nanotubes at the electrode interface: Towards highly efficient photovoltaic wires. *Adv. Mater.* **24**, 4623–4628 (2012).

Funding: We are grateful for the financial support from the U.S. Department of Defense Multidisciplinary University Initiative under AFOSR (FA9550-12-1-0037; J. Harrison, Program Manager), Case Western Reserve University–Wenzhou Medical University (CON115346), and Natural Science Foundation of China (51202167). **Competing interests:** The authors declare that they have no competing interests.

Submitted 11 December 2014
Accepted 16 June 2015
Published 4 September 2015
10.1126/sciadv.1400198

Citation: Y. Xue, Y. Ding, J. Niu, Z. Xia, A. Roy, H. Chen, J. Qu, Z. L. Wang, L. Dai, Rationally designed graphene-nanotube 3D architectures with a seamless nodal junction for efficient energy conversion and storage. *Sci. Adv.* **1**, 1400198 (2015).